Geophysical Research Letters

RESEARCH LETTER
10.1029/2021GL094470

Small-Scale Intraslab Heterogeneity Weakens Into the Mantle Transition Zone

Zhichao Shen[1], Zhongwen Zhan[1], and Jennifer M. Jackson[1]

[1]Seismological Laboratory, California Institute of Technology, Pasadena, CA, USA

Key Points:

- We apply inter-source interferometry to probe the small-scale intraslab heterogeneity in the mantle transition zone beneath the Japan Sea
- The deep intraslab scattering level needs to be weaker than at intermediate depth to fit the high-frequency interferometric waveforms
- The decrease of intraslab scattering with depth reveals the processes associated with slab dehydration

Supporting Information:

Supporting Information may be found in the online version of this article.

Correspondence to:

Z. Shen,
zshen@caltech.edu

Citation:

Shen, Z., Zhan, Z., & Jackson, J. M. (2021). Small-scale intraslab heterogeneity weakens into the mantle transition zone. *Geophysical Research Letters*, *48*, e2021GL094470. https://doi.org/10.1029/2021GL094470

Received 26 MAY 2021
Accepted 10 NOV 2021

Abstract Small-scale intraslab heterogeneity is well documented seismically in multiple subduction zones, but its nature remains elusive. Previous efforts have been mostly focusing on the scattering strength at intermediate depth (<350 km), without constraining its evolution as a function of depth. Here, we illustrate that the inter-source interferometry method, which turns deep earthquakes into virtual receivers, can resolve small-scale intraslab heterogeneity in the mantle transition zone. The interferometric waveform observations in the Japan subduction zone require weak scattering (<1.0%) within the slab below 410 km. Combining with previous studies that suggest high heterogeneity level (~2.5%) at intermediate depth, we conclude that the small-scale intraslab heterogeneity weakens as slabs subduct. We suggest that the heterogeneities are caused by intraslab hydrous minerals, and the decrease in their scattering strength with depth reveals processes associated with dehydration of subducting slabs.

Plain Language Summary Deep earthquakes often generate surprisingly lengthy surface shaking, due to wave trapping and guiding along laminar small-scale scatterers within subducting slabs. The nature of these scatterers is not well understood, although they have been observed in multiple subduction zones above 350 km. Here, by turning some deep earthquakes into virtual sensors closer to our target, we find that the small-scale scatterers within the slab core fade substantially as slab subducts, from ~2.5% above 350 km to <1% below 410 km. The fading signal suggests that the scatterers are caused by heterogeneous hydration of the slab in the outer rise that decreases as the slab core dehydrates.

1. Introduction

Multiscale seismic structures of subducting slabs provide fundamental constraints on the slab thermal and petrological properties. Extensive investigations have been conducted on the large- (>100 km) and intermediate-scale (10–100 km) slab structures. For example, subducting plates imaged from tomographic models are characterized as large-scale high-velocity anomalies descending into the mantle with complicated destinies (e.g., Fukao & Obayashi, 2013; Goes et al., 2017; Li et al., 2008; Lu et al., 2019; Ritsema et al., 2011; Simmons et al., 2012; Zhao, 2004). These high velocities are thought to be primarily temperature controlled and thus can be used to constrain the thermal-petrological state of the slab core (Cammarano et al., 2003; Zhan et al., 2014). On the intermediate scale, deterministic seismic waveform modeling suggests that distinct oceanic crusts remain to a depth of ~150 km globally with a velocity reduction up to 15%, implying a vigorous slab hydration process along the top of subducting plates (Abers, 2000; Abers et al., 2003; Garth & Rietbrock, 2014b, 2017; Omori et al., 2004; Savage, 2012). As another example of an intermediate-scale slab structure, low-velocity metastable olivine wedge (MOW), which consists of low-pressure olivine polymorphs within a cold slab in the mantle transition zone (MTZ), has been confirmed beneath the Japan Sea (Iidaka & Suetsugu, 1992). The recently revealed dimension of MOW supports transformational faulting as the initial mechanism of deep-focus earthquakes and a dry slab core (Shen & Zhan, 2020; Zhan, 2020).

In contrast to studies on the large and intermediate scales, small-scale (<10 km) slab structures have been mostly studied by stochastically modeling high-frequency scattered waves. To explain the high-frequency coda of long duration and large amplitude along the Japan trench from deep earthquakes, Furumura and Kennett (2005) proposed a laminar intraslab heterogeneity model after ruling out slab attenuation and hydrous oceanic crust as possible causes. The intraslab scatterers are described by a Von-Kármán distribution with a downdip correlation wavelength of 10 and 0.5 km in thickness with a velocity fluctuation of 2.5%. Since then, a similar heterogeneity level at intermediate depth (<350 km) has been suggested in a few other old subducting plates (Furumura & Kennett, 2008; Sun et al., 2014). Such stochastic structure is conjectured

to represent melt-rich shear bands or channels which initially formed near the mid-ocean ridge, preserved during the thickening of the oceanic plate and aligned to the horizontal direction by the relative shear mantle flow (Sun et al., 2014). Alternatively, Garth and Rietbrock (2014b) attributed the extended *P* wave coda to an elongated intraslab heterogeneity model oriented with an angle similar to the fault angles at the outer rise. In this manner, the fine-scale structures are associated with serpentinized faults that can penetrate deeper in the slab due to unbending forces and cycle a great amount of water into the mantle. Yet, given the limited seismological observations at intermediate depth range, there is no broadly accepted petrological understanding for the small-scale intraslab heterogeneity.

To interrogate the nature of these elongated scatterers, it may help to unveil their fate at larger depth using seismic scattering strength as an indicator. For example, the small-scale scatterers can be much weaker at depth due to the slab dehydration if they are located along (previously) hydrated faults. However, compared to intermediate depth, seismic signatures of intraslab heterogeneity in the MTZ are difficult to separate from the waveform complexities caused by the shallower slab, lithospheric, and crustal scattering (Chen et al., 2007), as well as deep slab structure MOW (Furumura et al., 2016). To address this challenge, we incorporate the MOW model from Shen and Zhan (2020) (hereafter referred as SZ20) and investigate intraslab heterogeneity using an inter-source interferometry method which has been shown effective in isolating deep slab signals. In this paper, we first validate the inter-source interferometry technique for small-scale intraslab heterogeneity with numerical simulations. Then, to explain the interferometric observations, we invoke different intraslab heterogeneity models in the MTZ beneath the Japan Sea. Combining previous studies for the intermediate depth range, we suggest that the intraslab scattering level decreases with depth and correlates with the process associated with slab dehydration.

2. Deep Slab Model for Inter-source Interferometry

Inter-receiver interferometry has been widely used to reconstruct the Green's function between receiver pairs given a diffusive seismic wavefield (Campillo & Paul, 2003; Shapiro et al., 2005). Similarly, due to the reciprocity theorem that interchanges the receivers and sources, the inter-source interferometry synthesizes the transient strain triggered by passing seismic waves from one source to the other (Curtis et al., 2009). This is as if we convert one of the earthquakes into a virtual "seismometer" and record the other event. The inter-source interferometry method has succeeded in retrieving the seismic response between earthquakes in both global (Curtis et al., 2009) and regional scales (Eulenfeld, 2020; Tonegawa & Nishida, 2010), providing unprecedented resolution in revealing the source-side velocity structure. In particular, for the subducting slab scenario, this novel approach can isolate the deep slab from shallow lithospheric structures by cross-correlating coda waves from deep earthquakes at common stations. Previously, with Hi-net data, SZ20 found that the inter-source interferometric waveforms from six deep earthquake pairs present coherent negative pulses at long period (0.2–2 Hz) while vary sharply at shorter period (0.2–5 Hz; Figure 1). After ruling out errors in the focal mechanism and signals related to the subducting crust, they confirmed the existence of MOW beneath the Japan Sea ~30-km thick at 410-km depth and gradually thinning to a depth of at least 580 km with a velocity reduction of 5% for *P* wave and 7% for *S* wave (Figure 1a).

Building on the SZ20 result, we construct the slab profile initially from a thermal model tuned for the Japan subduction zone (Moresi et al., 2007; Sdrolias & Müller, 2006) and implement a MOW delineated by a temperature contour of $T_{\mathrm{MOW}} = 664°\mathrm{C}$ within the slab below 410 km. To describe the small-scale heterogeneity, we adopt the Von-Kármán type autocorrelation function (ACF) given as (Sato et al., 2012)

$$P\left(k_x, k_z\right) = \frac{4\pi\kappa\varepsilon^2 a_x a_z}{\left(1 + a_x^2 k_x^2 + a_z^2 k_z^2\right)^{\kappa+1}} \tag{1}$$

where P is the power spectral density function and κ is the Hurst exponent set as 0.5 in this study. k_i is the wavenumber in ith direction, ε is the mean square fractional fluctuation, and a_x and a_z are the correlation distances in the orthogonal x (slab-parallel) and z (slab-normal) components, respectively. Note that the Von-Kármán type ACF is designed to describe a turbid scenario enriching short-scale components using a few parameters and thus cannot capture the full range of heterogeneity effects that may be present in the slab. To produce realistic coda on the surface stations, we incorporate isotropic heterogeneity with $a_x = a_z = 10$ km

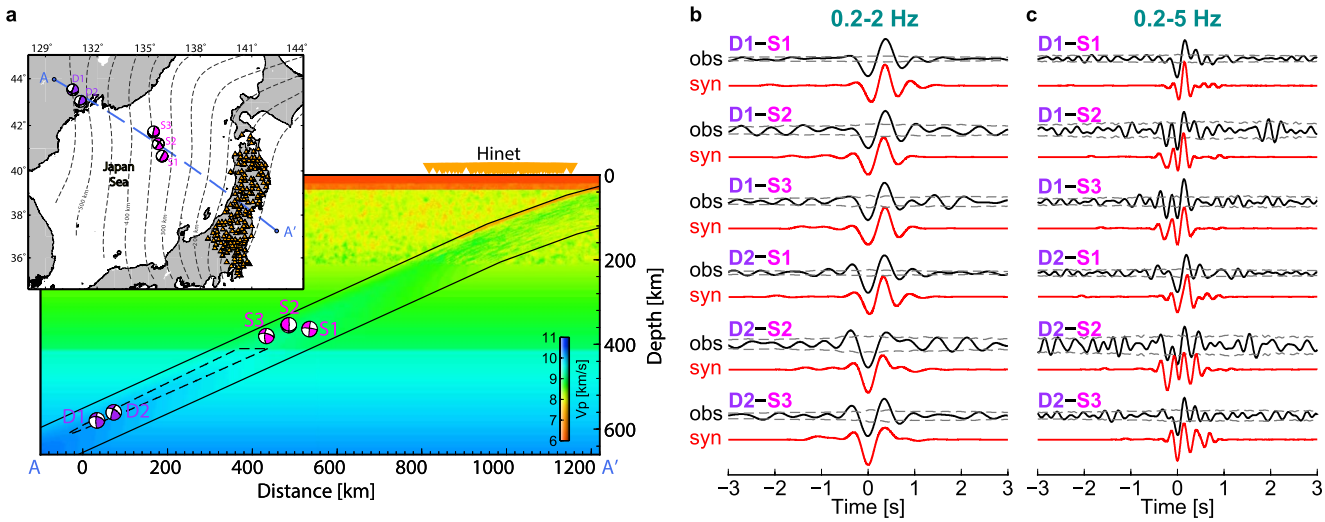

Figure 1. Metastable olivine wedge (MOW) model beneath the Japan Sea. (a) Map view of our studied region and the *P* wave velocity profile along AA′. The black solid and dashed lines denote the subducting Pacific slab (Hayes et al., 2018) and a MOW model beneath the Japan Sea (Shen & Zhan, 2020). Orange triangles are Hi-net stations used for inter-source interferometry. (b) 0.2–2 Hz and (c) 0.2–5 Hz waveform comparison between interferometric observations and synthetics (no scattering is imposed here) for all six deep earthquake pairs. The gray dashed lines denote the noise level.

and $\varepsilon = 2.0\%$ in the lithosphere (<210 km) and laminar intraslab scatterers with $a_x = 10$ km, $a_z = 0.5$ km, and $\varepsilon = 2.5\%$ at intermediate depth (70–350 km) following Furumura and Kennett (2005).

Guided by previous small-scale scatter studies for intermediate depths, we test a variety of intraslab heterogeneity models below 410 km. The heterogeneity models are simultaneously superimposed on our background *P* and *S* wave velocities and densities of the subducting slab and can be generally categorized into two groups (Melt-type and Fault-type) with different combinations of ACF parameters and the orientation of elongation (apparent dipping angle to the slab surface; Table S1 in Supporting Information S1). Melt-type models: slab-parallel scatterers with $a_x = 10$ km, $a_z = 0.5$ km, and a set of heterogeneity level ε ranging from 0.0% to 2.5% with an interval of 0.5% (Furumura & Kennett, 2005), which are referred to as Melt_constant models. We also linearly increase ε from the slab surface (0.5%) to the bottom (2.5%), termed the Melt_basal model. This strong basal heterogeneity model is proposed to resolve a discrepancy between seismological and experimental observations (Kennett & Furumura, 2015). Fault-type models: elongated scatterers with a dipping angle of 25° to the slab surface, $a_x = 10$ km, $a_z = 0.5$ km, and a set of constant heterogeneity level ε ranging from 0.0% to 2.5% with an interval of 0.5% (Garth & Rietbrock, 2014b), referred to as Fault_constant models. Once the slab model is set up, we simulate the seismic wavefield using a fully elastic GPU-based two-dimensional finite difference code (Li et al., 2014). With a grid spacing of 75 m and time steps of 0.001 s, the synthetic seismograms are accurate for frequencies up to 6 Hz.

3. Synthetic Test

With synthetic seismograms, we proceed to first validate the inter-source interferometry for small-scale intraslab scatterers. Figure 2a shows the 0.2–2 Hz benchmark result for the Melt_constant1.0 model ($\varepsilon = 1.0\%$) with earthquake pair D1–S1. The coda wave cross correlations of individual stations present coherent negative pulses at a constant arrival time (~54 s), suggesting a diffuse coda wavefield in the stationary phase zone. The negative polarity of the 2 Hz cross correlations, as demonstrated from SZ20, is the result of *P* wave reverberations within the low-velocity MOW. By averaging over all the cross correlations, the stacked interferometric waveform matches the directly simulated *P* wave strain seismograms from source D1 to virtual receiver S1 (Figure 2a, top panel). Following the same procedure, we also compare the stacked cross correlations to theoretical strain waveforms for other intraslab heterogeneity models. As shown in Figure 2 and Figure S1 in Supporting Information S1, the inter-source interferometry recovers the strain Green's function well at both 0.2–2 and 0.2–5 Hz in all scenarios, validating the applicability of inter-source interferometry for scattering slabs. Intriguingly, regardless of the type of intraslab heterogeneity, the long period (0.2–2 Hz)

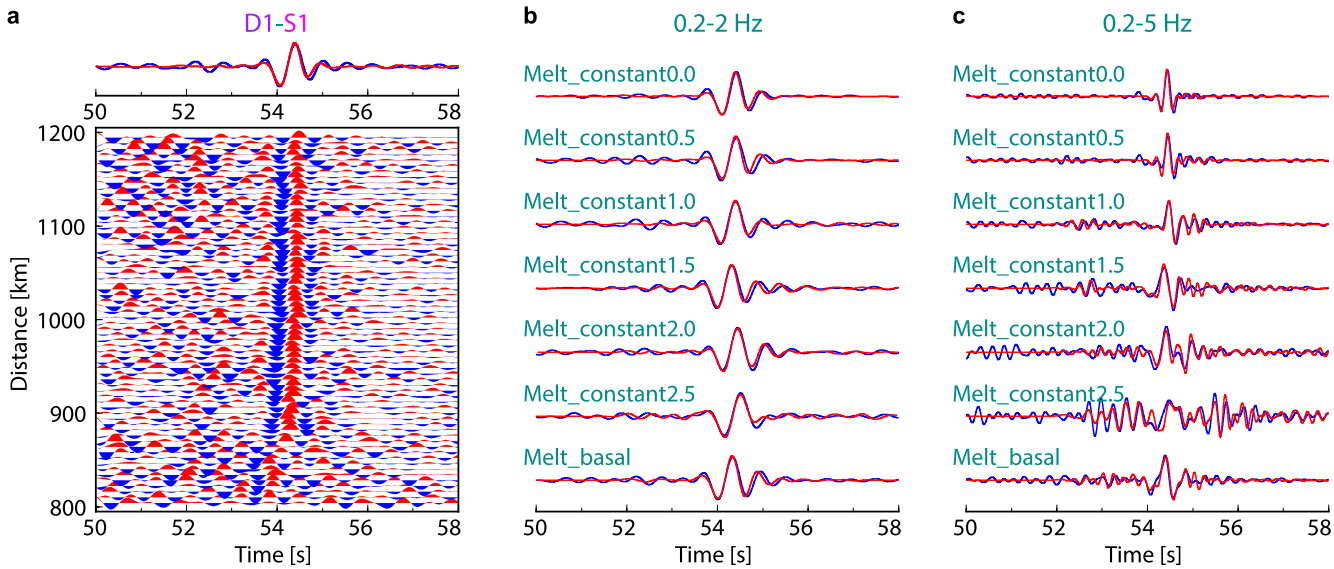

Figure 2. Inter-source interferometry synthetic benchmark for different intraslab heterogeneity models. (a) 0.2–2 Hz inter-source interferometry benchmark result for the Melt_constant1.0 model ($\varepsilon = 1.0\%$) with D1–S1 pair. The lower panel shows the cross-correlation record section. The upper panel is the waveform comparison between stacked cross correlation (blue) and theoretical strain response (red). (b) 0.2–2 Hz waveform comparison between the stacked cross correlations (blue) and theoretical strain responses (red) for Melt-type models with D1–S1 pair. (c) Similar to (b) but for 0.2–5 Hz.

interferometric waveforms do not differ substantially in waveform shape, confirming that the MOW (the controlling factor in this frequency band) is required to fit the inter-source interferometric observations in Japan (Figure 1b; Shen & Zhan, 2020). Moreover, the arrival time differences among all the 0.2–2 Hz interferometric signals are less than 0.2 s, which is within the earthquake location uncertainty. Hence, we solely focus on interpreting the waveform shape in this study. In contrast, the intraslab heterogeneity level ε strongly affects the high-frequency (0.2–5 Hz) waveforms. For instance, weak scattering models (e.g., Melt_constant0.5) present simple pulses, whereas strong scattering cases (e.g., Melt_constant2.5) exhibit lengthy wave trains (Figure 2c). Compared to Melt models, the Fault-type models show similar waveform variations but less complicated for the heterogeneity level ε larger than 1.5% (Figure S1b in Supporting Information S1). This is probably because the dipping configuration of laminate scatterers is less effective in trapping the high-frequency signals along the raypath from D1 to S1. Overall, the elongated small-scale heterogeneity acts as a frequency selective waveform modulator that weakly perturbs the low frequency but efficiently channels the high-frequency energy, which is consistent with previous seismic observations (Furumura & Kennett, 2005). Therefore, the 5 Hz interferometric waveforms are crucial to constrain the small-scale intraslab heterogeneity in MTZ.

4. Result

Having shown the sensitivity of inter-source interferometry to small-scale intraslab scatterers, we compute the synthetic seismograms of all six deep earthquake pairs for different heterogeneity models (Figure 3 and Figure S2 in Supporting Information S1) and compare them to the interferometric waveforms obtained by SZ20. Similar to the benchmark tests above, the high-frequency strain waveform complexity of D1-S1 pair correlates with the scattering strength (ε) for the Melt-type models but shows little dependencies on heterogeneity level of the Fault-type models (Figure 3a). Even so, the simple waveforms for strong Fault-type scattering cases contradict the observations with nearly opposite waveform shapes. As for the D1-S2 and D1-S3 pairs, both Melt- and Fault-type models with large ε introduce lengthy coda or secondary arrivals at 5 Hz, failing to capture the interferometric observations which exhibit "W-shape" waveforms (two negative wiggles preceding a positive one; Figures 3b and 3c). Note that the Melt_constant1.0/1.5 and Melt_basal models yield better fit to the D1–S3 observation than the Melt_constant0.5 case but perform worse for D1-S1/S2 and D2-S1 pairs (Figure 3 and Figure S2 in Supporting Information S1). Thus, in general, increasing

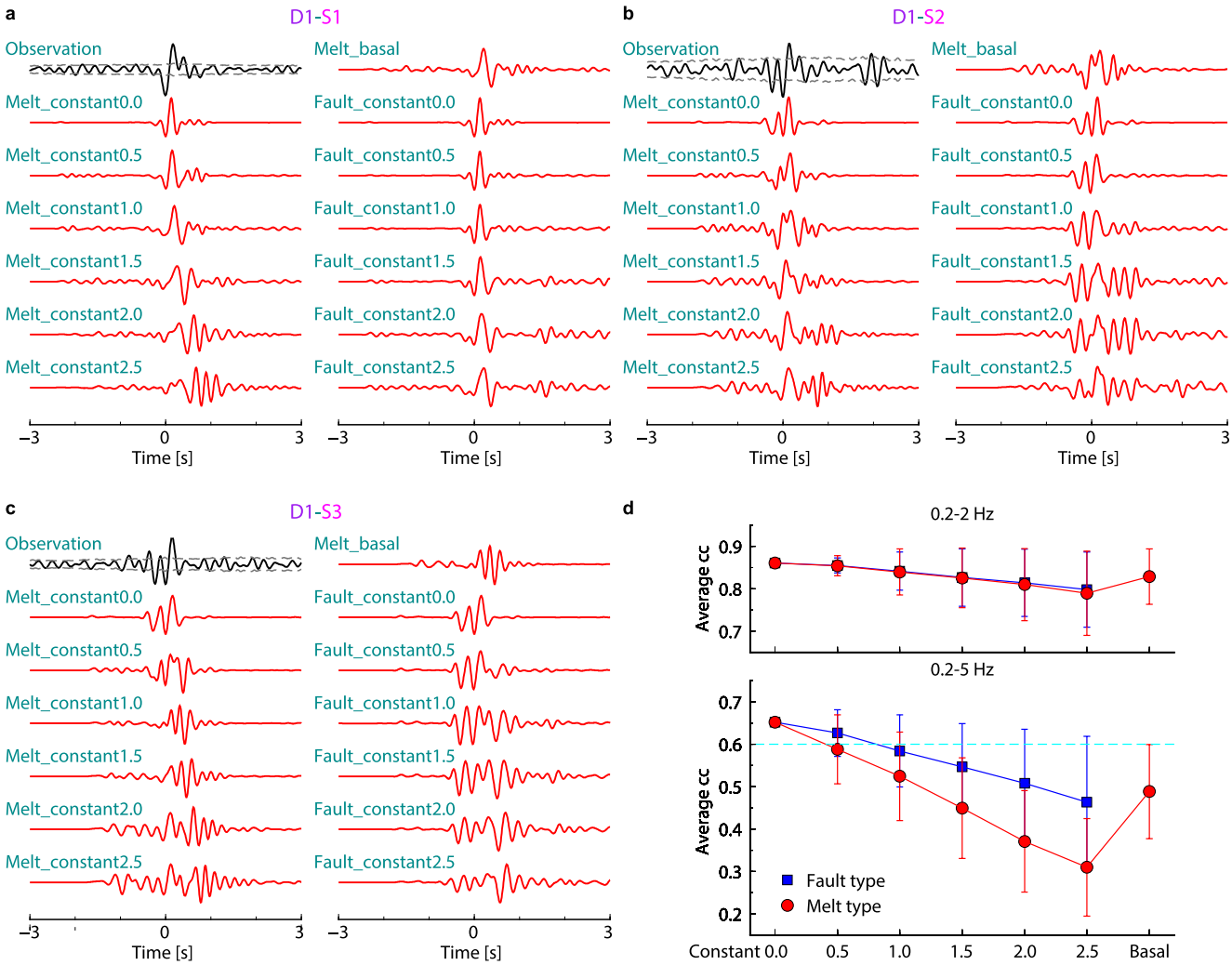

Figure 3. Data suggest weak intraslab heterogeneity level below 410 km. 0.2–5 Hz waveform comparisons between inter-source interferometric observations (black) and synthetic strain waveforms (red) of Melt- and Fault-type heterogeneity models for (a) D1-S1 pair, (b) D1-S2 pair, and (c) D1-S3 pair in one realization. (d) Average cross-correlation coefficients (cc) of all six event pairs between observations and synthetics for Melt-type (red circles) and Fault-type (blue squares) heterogeneity models. The error bars indicate the 95% confidence interval, and the cyan dashed line denotes a cc threshold of 0.6.

the heterogeneity level reduces the overall similarity between interferometric observations and synthetic seismograms.

In fact, because of the stochastic nature of small-scale scatterers, the 5 Hz waveforms can vary substantially in a set of realizations of the same intraslab heterogeneity types with $\varepsilon > 1.5\%$ (Figure S3 in Supporting Information S1). To statistically quantify the effect of random media on the waveform fitting, we conduct 100 realizations for each intraslab heterogeneity type. In each realization, we cross correlate the synthetics with observed interferometric waveforms in a 6-s time window and average the six cross-correlation coefficients (cc) by signal to noise ratios to represent the similarity between observations and simulations. For each intraslab heterogeneity type, the distribution of averaged cc can be approximated by a Gaussian distribution (Figure S4 in Supporting Information S1). As shown in Figure 3d, the mean value of averaged cc slightly drops from 0.88 ($\varepsilon = 0.0\%$) to 0.80 ($\varepsilon = 2.5\%$) at 0.2–2 Hz for both Melt- and Fault-type models. Whereas the averaged cc for 0.2–5 Hz starts at a lower value of 0.65 possibly due to elevated observational noise level and decreases dramatically to 0.46 and 0.30 for the Fault_constant2.5 and Melt_constant2.5 models, respectively. The performance of the Melt_basal case falls between the Melt_constant1.0 and Melt_constant1.5. Due to the slab-parallel raypaths of the six earthquake pairs (Figure 1), the 5 Hz waveforms are more sensitive to the Melt-type models than the Fault-type models. By defining a cc threshold value of 0.6 that corresponds

to a 10% fit reduction from the non-scattering model, we assess the probability of achieving the proper waveform fit to observations for each intraslab heterogeneity type. The resulting probability reduces abruptly to less than 10% when ε is larger than 1.0% and 1.5% for the Melt- and Fault-type, respectively (Figure S5 in Supporting Information S1), rejecting the strong scattering model at depth. Moreover, the probability of Melt_constant0.5 and Fault_constant1.0 models does not exceed 30% (Figure S5 in Supporting Information S1), thus the upper bound of the intraslab heterogeneity level below 410 km is probably less than 0.5% and 1.0% for the Melt- and Fault-type models, respectively.

5. Discussion

5.1. Reduced Intraslab Scattering at Depth

In this study, we are restricted to 2D simulations because of the computational cost for 3D. Generally, 2D simulation of seismic wave propagation shows different features of the 3D case due to differences in Green's function and geometrical spreading. Nevertheless, the seismic wavefield in our 2D simulations is mostly trapped waves within the MOW and scatterers. Previous studies of high-frequency waves show that differences in effects of trapping are not so significant between 2D and 3D simulations (Furumura & Kennett, 2005; Garth & Rietbrock, 2014a; Takemura et al., 2015). Therefore, our 2D slab model can represent the general feature of intraslab scatterers within the updip dimension. Still, without comprehensive 3D simulations, we cannot fully understand the character of intraslab scatterers, such as the presence of strong azimuthal-dependent scatterers (Furumura & Kennett, 2021). Note that the frequency contents of our interferometric observations are narrow-banded due to the small magnitudes of deep earthquakes. Nonetheless, increasing the small-scale intraslab heterogeneity level raises the high-frequency strain waveform complexity. For simultaneously fitting the six inter-source interferometric observations which all present distinct signals, the intraslab scattering level (ε) is preferred to be less than 1.0%. To further reinforce our argument, we investigate the potential influence of MOW geometry as defined by different slab thermal structures. Two cases are examined here: one with slightly thinner MOW produces reasonable overall waveform fits without scatterers, while the other case with thicker MOW presents similar waveform fit at 0.2–2 Hz but poorly fits the 0.2–5 Hz observations without scatterers (Figure S6 in Supporting Information S1). Similar to Figure 3d, the cross-correlation coefficients for both scenarios slightly drop at 0.2–2 Hz but dramatically decrease with the heterogeneity level at 0.2–5 Hz, confirming the robustness of the previously proposed MOW model by SZ20 and a weakly scattering slab in the MTZ (Figure S6 in Supporting Information S1). On the other hand, previous studies have suggested a laminar intraslab heterogeneity with strong scattering ($\varepsilon = 2.5\%$) at intermediate depth range for the Japan subduction zone by fitting long-duration coda (Furumura & Kennett, 2005; Garth & Rietbrock, 2014b). Our reduced intraslab heterogeneity model also reproduces the coda features observed near the trench (Figure S7 in Supporting Information S1). In fact, the coda characteristics are predominated by the low-velocity MOW and shallower scattering (Furumura et al., 2016). Therefore, we propose that the elongated intraslab heterogeneity decreases from 2.5% to <1.0% in the MTZ beneath the Japan Sea (Figure 4).

5.2. Interpretation for the Origin of Intraslab Scatterers

At face value, the reduced heterogeneity level at depth (i.e., decreased seismic visibility) may appear challenging to interpret. However, as discussed above, there is strong evidence for the presence of a MOW at these depths and observations of stronger scattering at shallower depths. Thus, we have a depth trend for which we can attempt to understand. That is, there is a decreasing trend in seismic scatterers with increasing depth to the MTZ, and this trend is resolved for the lithospheric section (core) of the slab. The presence of low-velocity anomalies in the crustal portion of the slab (e.g., hydrous phases) always generates positive polarities of interferometric waveforms at 0.2–2 Hz, contradicting our observed negative polarities (Figure S8 in Supporting Information S1). This reinforces that our observations are dominated by the seismic structures in the slab core and have little sensitivity to the slab crust. Therefore, we cannot rule out the possibility of slab crustal complexity.

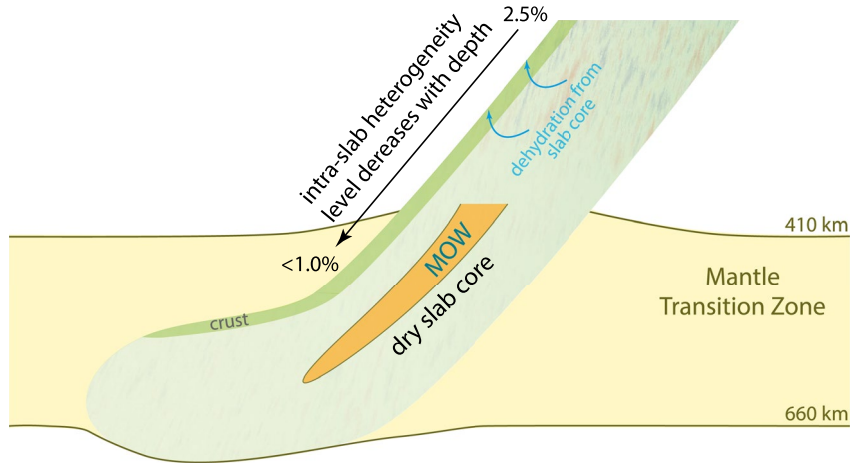

Figure 4. Cartoon of intraslab heterogeneity level with depth beneath the Japan Sea. The strong scattering of 2.5% at intermediate depth and the MOW are suggested by Furumura and Kennett (2005) and SZ20, respectively. If a MOW is only stabilized by an anhydrous phase assemblage (Du Frane et al., 2013), then the decrease of scattering strength toward greater depth (this study) in combination with the above-mentioned constraints indicates that we are capturing processes associated with slab dehydration.

5.2.1. Melt Bands

It has been suggested that the presence of preserved (and potentially re-activated) melt-bands could explain the strong *P* wave coda at intermediate depths (Furumura & Kennett, 2008; Sun et al., 2014). To explain the current set of observations here, one would infer that these preserved melt bands would become seismically invisible in the MTZ. Although this is a reasonable hypothesis, the existence and preservation of such melt-rich bands or channels at the kilometer scale along subducting slabs require corroborating observations, such as observations at shallower depths and co-located strong intraslab anisotropy, as the petrological evidence of melt band lamination have only been derived from experimental and modeling work and are mostly at the micrometer scale (Katz et al., 2006).

5.2.2. Hydrated Faults

At the Japan trench, plate bending stress creates pervasive fractures and faults extending to the oceanic lithosphere (Fujie et al., 2016, 2018; Obana et al., 2019), promoting water penetration in the deeper slab and mantle serpentinization prior to subduction (Faccenda et al., 2009; Iyer et al., 2012). The intraslab seismic scatterers at intermediate depths along this slab (Furumura & Kennett, 2005) could therefore be explained by the short-scale serpentinized faults (Garth & Rietbrock, 2014b). As the slab subducts, the elevated pressure and temperature lead to a series of breakdown reactions of hydrous minerals, expelling aqueous fluid to refertilize the mantle wedge (van Keken et al., 2011). The water released from serpentinite breakdown can progressively percolate upward along an intraslab layer characterized by the tectonic stress gradient (Faccenda et al., 2012). For cold slabs like the Japan subduction zone, the serpentinites could transform to hydrous dense magnesium silicates (HDMS) below the subarc depth (Chen et al., 2019; Faccenda, 2014). Given the existence of a MOW (Shen & Zhan, 2020) which requires an extremely dry slab core (<75 wt ppm; Du Frane et al., 2013; Kawakatsu & Yoshioka, 2011) and the lack of intraslab *P* wave coda in the MTZ (this study), the dehydration process of the slab core is almost complete by 410 km. This would imply that HDMS such as clinohumite could possibly transport "water" into MTZ only along the slab top (Stalder & Ulmer, 2001). As mentioned above, we cannot rule out the presence of a hydrous-rich slab crust. Rather our observations shed light on the dehydration process of slab cores that could lead to (re-)hydration of the slab crust and formation of dense oxyhydroxide phases (e.g., Buchen et al., 2021; Karato, 2006; Ohira et al., 2019; Ohtani, 2020).

6. Conclusion

In this study, we applied inter-source interferometry method to constrain the small-scale intraslab scatterers below 410 km beneath the Japan Sea. By conducting numerical simulations for various intraslab heterogeneity scenarios, we validated the robustness of previously proposed MOW model by Shen and Zhan (2020) and found that strong scattering models tend to complicate the high-frequency waveforms, leading to a worse fit to the interferometric observations. We quantified the intraslab heterogeneity level to be less than 1.0% below 410 km. Combining with previous observations of strong scattering (~2.5%) at intermediate depths, we conclude that the intraslab heterogeneity weakens as the slab subducts. Given the pervasive faults extending to the oceanic lithosphere at the Japan trench and the existence of a MOW in the MTZ, we suggest that the small-scale scatterers are caused by hydration processes in the outer rise. The observed weakening of scattering strength reveals that the dehydration process of the slab core must be complete by 410 km and could possibly lead to (re-)hydration of the slab crust and formation of dense oxyhydroxide phases.

Data Availability Statement

Seismic data are collected from Hi-net (www.hinet.bosai.go.jp) and F-net (www.fnet.bosai.go.jp). The earthquake catalog and focal mechanisms are downloaded from ISC-EHB distributed by the International Seismological Centre (http://www.isc.ac.uk/isc-ehb/) and National Research Institute for Earth Science and Disaster Resilience (NIED; https://www.fnet.bosai.go.jp/event/search.php?LANG=en).

Acknowledgments
The authors are grateful to Mike Gurnis, Rob Clayton, and two anonymous reviewers for discussions and suggestions. The authors are grateful to the National Science Foundation's (NSF) Collaborative Study of Earth's Deep Interior under EAR-2009935 for support of this work.

References

Abers, G. A. (2000). Hydrated subducted crust at 100–250 km depth. *Earth and Planetary Science Letters*, *176*(3), 323–330. https://doi.org/10.1016/s0012-821x(00)00007-8

Abers, G. A., Plank, T., & Hacker, B. R. (2003). The wet Nicaraguan slab. *Geophysical Research Letters*, *30*(2), 1098. https://doi.org/10.1029/2002GL015649

Buchen, J., Sturhahn, W., Ishii, T., & Jackson, J. M. (2021). Vibrational anisotropy of δ-(Al, Fe)OOH single crystals as probed by nuclear resonant inelastic X-ray scattering. *European Journal of Mineralogy*, *33*(4), 485–502. https://doi.org/10.5194/ejm-33-485-2021

Cammarano, F., Goes, S., Vacher, P., & Giardini, D. (2003). Inferring upper-mantle temperatures from seismic velocities. *Physics of the Earth and Planetary Interiors*, *138*(3–4), 197–222. https://doi.org/10.1016/s0031-9201(03)00156-0

Campillo, M., & Paul, A. (2003). Long-range correlations in the diffuse seismic coda. *Science*, *299*(5606), 547–549. https://doi.org/10.1126/science.1078551

Chen, M., Manea, V. C., Niu, F., Wei, S. S., & Kiser, E. (2019). Genesis of intermediate-depth and deep intraslab earthquakes beneath Japan constrained by seismic tomography, seismicity, and thermal modeling. *Geophysical Research Letters*, *46*, 2025–2036. https://doi.org/10.1029/2018GL080025

Chen, M., Tromp, J., Helmberger, D., & Kanamori, H. (2007). Waveform modeling of the slab beneath Japan. *Journal of Geophysical Research*, *112*, B02305. https://doi.org/10.1029/2006JB004394

Curtis, A., Nicolson, H., Halliday, D., Trampert, J., & Baptie, B. (2009). Virtual seismometers in the subsurface of the Earth from seismic interferometry. *Nature Geoscience*, *2*(10), 700–704. https://doi.org/10.1038/ngeo615

Du Frane, W. L., Sharp, T. G., Mosenfelder, J. L., & Leinenweber, K. (2013). Ringwoodite growth rates from olivine with ~75 ppmw H_2O: Metastable olivine must be nearly anhydrous to exist in the mantle transition zone. *Physics of the Earth and Planetary Interiors*, *219*, 1–10. https://doi.org/10.1016/j.pepi.2013.04.001

Eulenfeld, T. (2020). Toward source region tomography with intersource interferometry: Shear wave velocity from 2018 West Bohemia swarm earthquakes. *Journal of Geophysical Research: Solid Earth*, *125*, e2020JB019931. https://doi.org/10.1029/2020JB019931

Faccenda, M. (2014). Water in the slab: A trilogy. *Tectonophysics*, *614*, 1–30. https://doi.org/10.1016/j.tecto.2013.12.020

Faccenda, M., Gerya, T. V., & Burlini, L. (2009). Deep slab hydration induced by bending-related variations in tectonic pressure. *Nature Geoscience*, *2*(11), 790–793. https://doi.org/10.1038/ngeo656

Faccenda, M., Gerya, T. V., Mancktelow, N. S., & Moresi, L. (2012). Fluid flow during slab unbending and dehydration: Implications for intermediate-depth seismicity, slab weakening and deep water recycling. *Geochemistry, Geophysics, Geosystems*, *13*, Q01010. https://doi.org/10.1029/2011GC003860

Fujie, G., Kodaira, S., Kaiho, Y., Yamamoto, Y., Takahashi, T., Miura, S., & Yamada, T. (2018). Controlling factor of incoming plate hydration at the north-western Pacific margin. *Nature Communications*, *9*(1), 1–7. https://doi.org/10.1038/s41467-018-06320-z

Fujie, G., Kodaira, S., Sato, T., & Takahashi, T. (2016). Along-trench variations in the seismic structure of the incoming Pacific plate at the outer rise of the northern Japan Trench. *Geophysical Research Letters*, *43*, 666–673. https://doi.org/10.1002/2015GL067363

Fukao, Y., & Obayashi, M. (2013). Subducted slabs stagnant above, penetrating through, and trapped below the 660 km discontinuity. *Journal of Geophysical Research: Solid Earth*, *118*, 5920–5938. https://doi.org/10.1002/2013JB010466

Furumura, T., Kennett, B. L., & Padhy, S. (2016). Enhanced waveguide effect for deep-focus earthquakes in the subducting Pacific slab produced by a metastable olivine wedge. *Journal of Geophysical Research: Solid Earth*, *121*, 6779–6796. https://doi.org/10.1002/2016JB013300

Furumura, T., & Kennett, B. L. N. (2005). Subduction zone guided waves and the heterogeneity structure of the subducted plate: Intensity anomalies in northern Japan. *Journal of Geophysical Research*, *110*, B10302. https://doi.org/10.1029/2004JB003486

Furumura, T., & Kennett, B. L. N. (2008). A scattering waveguide in the heterogeneous subducting plate. *Advances in Geophysics*, *50*, 195–217. https://doi.org/10.1016/s0065-2687(08)00007-1

Furumura, T., & Kennett, B. L. N. (2021). Azimuthal variation of lithospheric heterogeneity in the northwest Pacific inferred from Po/So propagation characteristics and anomalously large ground motion of deep in-slab earthquakes. *Journal of Geophysical Research: Solid Earth*, *126*, e2021JB021717. https://doi.org/10.1029/2021JB021717

Garth, T., & Rietbrock, A. (2014a). Downdip velocity changes in subducted oceanic crust beneath Northern Japan—Insights from guided waves. *Geophysical Journal International*, *198*(3), 1342–1358. https://doi.org/10.1093/gji/ggu206

Garth, T., & Rietbrock, A. (2014b). Order of magnitude increase in subducted H_2O due to hydrated normal faults within the Wadati–Benioff zone. *Geology*, *42*(3), 207–210. https://doi.org/10.1130/g34730.1

Garth, T., & Rietbrock, A. (2017). Constraining the hydration of the subducting Nazca plate beneath Northern Chile using subduction zone guided waves. *Earth and Planetary Science Letters*, *474*, 237–247. https://doi.org/10.1016/j.epsl.2017.06.041

Goes, S., Agrusta, R., van Hunen, J., & Garel, F. (2017). Subduction-transition zone interaction: A review. *Geosphere*, *13*(3), 644–664. https://doi.org/10.1130/ges01476.1

Hayes, G. P., Moore, G. L., Portner, D. E., Hearne, M., Flamme, H., Furtney, M., & Smoczyk, G. M. (2018). Slab2, a comprehensive subduction zone geometry model. *Science*, *362*(6410), 58–61. https://doi.org/10.1126/science.aat4723

Iidaka, T., & Suetsugu, D. (1992). Seismological evidence for metastable olivine inside a subducting slab. *Nature*, *356*(6370), 593–595.

Iyer, K., Rüpke, L. H., Phipps Morgan, J., & Grevemeyer, I. (2012). Controls of faulting and reaction kinetics on serpentinization and double Benioff zones. *Geochemistry, Geophysics, Geosystems*, *13*, Q09010. https://doi.org/10.1029/2012GC004304

Karato, S. I. (2006). Remote sensing of hydrogen in Earth's mantle. *Reviews in Mineralogy and Geochemistry*, *62*(1), 343–375. https://doi.org/10.2138/rmg.2006.62.15

Katz, R. F., Spiegelman, M., & Holtzman, B. (2006). The dynamics of melt and shear localization in partially molten aggregates. *Nature*, *442*(7103), 676–679. https://doi.org/10.1038/nature05039

Kawakatsu, H., & Yoshioka, S. (2011). Metastable olivine wedge and deep dry cold slab beneath southwest Japan. *Earth and Planetary Science Letters*, *303*(1–2), 1–10. https://doi.org/10.1016/j.epsl.2011.01.008

Kennett, B. L. N., & Furumura, T. (2015). Toward the reconciliation of seismological and petrological perspectives on oceanic lithosphere heterogeneity. *Geochemistry, Geophysics, Geosystems*, *16*, 3129–3141. https://doi.org/10.1002/2015GC006017

Li, C., van der Hilst, R. D., Engdahl, E. R., & Burdick, S. (2008). A new global model for *P* wave speed variations in Earth's mantle. *Geochemistry, Geophysics, Geosystems*, *9*, Q05018. https://doi.org/10.1029/2007GC001806

Li, D., Helmberger, D., Clayton, R. W., & Sun, D. (2014). Global synthetic seismograms using a 2-D finite-difference method. *Geophysical Journal International*, *197*(2), 1166–1183. https://doi.org/10.1093/gji/ggu050

Lu, C., Grand, S. P., Lai, H., & Garnero, E. J. (2019). TX2019slab: A new *P* and *S* tomography model incorporating subducting slabs. *Journal of Geophysical Research: Solid Earth*, *124*, 11549–11567. https://doi.org/10.1029/2019JB017448

Moresi, L., Quenette, S., Lemiale, V., Meriaux, C., Appelbe, B., & Mühlhaus, H. B. (2007). Computational approaches to studying non-linear dynamics of the crust and mantle. *Physics of the Earth and Planetary Interiors*, *163*(1–4), 69–82. https://doi.org/10.1016/j.pepi.2007.06.009

Obana, K., Fujie, G., Takahashi, T., Yamamoto, Y., Tonegawa, T., Miura, S., & Kodaira, S. (2019). Seismic velocity structure and its implications for oceanic mantle hydration in the trench–outer rise of the Japan Trench. *Geophysical Journal International*, *217*(3), 1629–1642. https://doi.org/10.1093/gji/ggz099

Ohira, I., Jackson, J. M., Solomatova, N. V., Sturhahn, W., Finkelstein, G. J., Kamada, S., et al. (2019). Compressional behavior and spin state of δ-(Al, Fe)OOH at high pressures. *American Mineralogist*, *104*(9), 1273–1284. https://doi.org/10.2138/am-2019-6913

Ohtani, E. (2020). The role of water in Earth's mantle. *National Science Review*, *7*(1), 224–232. https://doi.org/10.1093/nsr/nwz071

Omori, S., Komabayashi, T., & Maruyama, S. (2004). Dehydration and earthquakes in the subducting slab: Empirical link in intermediate and deep seismic zones. *Physics of the Earth and Planetary Interiors*, *146*(1–2), 297–311. https://doi.org/10.1016/j.pepi.2003.08.014

Ritsema, J., Deuss, A. A., Van Heijst, H. J., & Woodhouse, J. H. (2011). S40RTS: A degree-40 shear-velocity model for the mantle from new Rayleigh wave dispersion, teleseismic traveltime and normal-mode splitting function measurements. *Geophysical Journal International*, *184*(3), 1223–1236. https://doi.org/10.1111/j.1365-246x.2010.04884.x

Sato, H., Fehler, M. C., & Maeda, T. (2012). *Seismic wave propagation and scattering in the heterogeneous Earth* (Vol. 496). Springer.

Savage, B. (2012). Seismic constraints on the water flux delivered to the deep Earth by subduction. *Geology*, *40*(3), 235–238. https://doi.org/10.1130/g32499.1

Sdrolias, M., & Müller, R. D. (2006). Controls on back-arc basin formation. *Geochemistry, Geophysics, Geosystems*, *7*, Q04016. https://doi.org/10.1029/2005GC001090

Shapiro, N. M., Campillo, M., Stehly, L., & Ritzwoller, M. H. (2005). High-resolution surface-wave tomography from ambient seismic noise. *Science*, *307*(5715), 1615–1618. https://doi.org/10.1126/science.1108339

Shen, Z., & Zhan, Z. (2020). Metastable olivine wedge beneath the Japan Sea imaged by seismic interferometry. *Geophysical Research Letters*, *47*, e2019GL085665. https://doi.org/10.1029/2019GL085665

Simmons, N. A., Myers, S. C., Johannesson, G., & Matzel, E. (2012). LLNL-G3Dv3: Global *P* wave tomography model for improved regional and teleseismic travel time prediction. *Journal of Geophysical Research*, *117*, B10302. https://doi.org/10.1029/2012JB009525

Stalder, R., & Ulmer, P. (2001). Phase relations of a serpentine composition between 5 and 14 GPa: Significance of clinohumite and phase E as water carriers into the transition zone. *Contributions to Mineralogy and Petrology*, *140*(6), 670–679. https://doi.org/10.1007/s004100000208

Sun, D., Miller, M. S., Agostinetti, N. P., Asimow, P. D., & Li, D. (2014). High frequency seismic waves and slab structures beneath Italy. *Earth and Planetary Science Letters*, *391*, 212–223. https://doi.org/10.1016/j.epsl.2014.01.034

Takemura, S., Yoshimoto, K., & Tonegawa, T. (2015). Scattering of trapped *P* and *S* waves in the hydrated subducting crust of the Philippine Sea plate at shallow depths beneath the Kanto region, Japan. *Geophysical Supplements to the Monthly Notices of the Royal Astronomical Society*, *203*(3), 2261–2276. https://doi.org/10.1093/gji/ggv423

Tonegawa, T., & Nishida, K. (2010). Inter-source body wave propagations derived from seismic interferometry. *Geophysical Journal International*, *183*(2), 861–868. https://doi.org/10.1111/j.1365-246x.2010.04753.x

van Keken, P. E., Hacker, B. R., Syracuse, E. M., & Abers, G. A. (2011). Subduction factory: 4. Depth-dependent flux of H_2O from subducting slabs worldwide. *Journal of Geophysical Research*, *116*, B01401. https://doi.org/10.1029/2010JB007922

Zhan, Z. (2020). Mechanisms and implications of deep earthquakes. *Annual Review of Earth and Planetary Sciences*, *48*, 147–174. https://doi.org/10.1146/annurev-earth-053018-060314

Zhan, Z., Helmberger, D. V., & Li, D. (2014). Imaging subducted slab structure beneath the Sea of Okhotsk with teleseismic waveforms. *Physics of the Earth and Planetary Interiors*, *232*, 30–35. https://doi.org/10.1016/j.pepi.2014.03.008

Zhao, D. (2004). Global tomographic images of mantle plumes and subducting slabs: Insight into deep Earth dynamics. *Physics of the Earth and Planetary Interiors*, *146*(1–2), 3–34. https://doi.org/10.1016/j.pepi.2003.07.032